Department of Physics Publications

Department of Physics

12-23-2008

Self-consistent calculations of strain-induced band gap changes in semiconducting (n, 0) carbon nanotubes

Pavan Kumar Valavala
Michigan Technological University

Douglas R. Banyai
Michigan Technological University

Max Seel
Michigan Technological University

Ranjit Pati
Michigan Technological University

Recommended Citation

Valavala, P. K., Banyai, D. R., Seel, M., & Pati, R. (2008). Self-consistent calculations of strain-induced band gap changes in semiconducting (n, 0) carbon nanotubes. *American Physical Society, 78*. http://dx.doi.org/10.1103/PhysRevB.78.235430
Retrieved from: https://digitalcommons.mtu.edu/physics-fp/123

Self-consistent calculations of strain-induced band gap changes in semiconducting (*n*,0) carbon nanotubes

Pavan K. Valavala, Douglas Banyai, Max Seel, and Ranjit Pati

Department of Physics, Michigan Technological University, Houghton, Michigan 49931, USA

First-principles density-functional calculations of the electronic structure, energy band gaps (E_g), and strain-induced band gap changes in moderate-gap single-walled (*n*,0) carbon nanotubes (SWNTs) are presented. It is confirmed that (*n*,0) SWNTs fall into two classes depending upon *n* mod 3=1 or 2. E_g is always lower for "mod 1" than for "mod 2" SWNTs of similar diameter. For *n* < 10, strong curvature effects dominate E_g; from *n*=10 to 17, the E_g oscillations, amplified due to σ-π mixing, decrease and can be explained very well with a tight-binding model which includes *trigonal warping*. Under strain, the two families of semiconducting SWNTs are distinguished by equal and opposite energy shifts for these gaps. For (10,0) and (20,0) tubes, the potential surface and band gap changes are explored up to approximately ±6% strain or compression. For each strain value, full internal geometry relaxation is allowed. The calculated band gap changes are ±(115±10) meV per 1% strain, positive for the mod 1 and negative for the mod 2 family, about 10% *larger* than the tight-binding result of ±97 meV and twice as large as the shift predicted from a tight-binding model that includes internal sublattice relaxation.

I. INTRODUCTION

A single-walled carbon nanotube (SWNT) is a one-dimensional (1D) nanostructured material, which has been the focal point of research over the past decade for intriguing applications ranging from nanoelectronics to biological sensors. The geometry of the SWNT is described by a chiral vector $(\vec{C})$: $\vec{C}=n\vec{a}+m\vec{b}$, denoted by (*n*,*m*) that connects the two crystallographically equivalent sites on the graphene sheet. Soon after their discovery and characterization,[1] the potential of this tubular structure was realized by theoretical work,[2–6] which showed that SWNTs can be categorized into three types: metallic, small gap, and moderate-gap semiconducting based on their chirality. It was proposed that a SWNT would exhibit metallic character if (*n*−*m*)/3 is an integer and a moderate-gap semiconductor in all other cases. Furthermore, these early tight-binding calculations also predicted that the gap E_g in a semiconducting SWNT is inversely proportional to its diameter (*d*) (Ref. 7) and monotonically decreases with the increase in diameter of the tube. This unique dependence of electronic properties of SWNTs on their diameter and chirality spawned a great interest in this material. This was later confirmed by the pioneering experimental work that measured electronic properties of SWNT.[8–11] These experiments probed the explicit dependence of chirality and diameter on the electronic properties and confirmed the earlier theoretical predictions with accuracy of ±0.05 nm in measured diameter and ±0.3 eV in measured E_g.

However, over the years, conflicting relationships have been reported on the exact dependence of E_g of the SWNTs on their diameter. Previous conclusions about monotonic 1/*d* dependence law have been challenged. For smaller *n* the trigonal shape of the equienergy lines around the **K** point of the graphene Brillouin zone (BZ) ("trigonal warping"[12]) needs to be taken into account. It was shown that a third-order Taylor expansion of the energy dispersion relation

around **K** point leads to an equation for E_g,[13] which depends on the chirality of the tube (generalized expression was given later[14]). The modified dispersion relation reflects the fact that the corresponding transitions for "mod 1" and "mod 2" nanotubes lie on different sides of the **K** point. Subsequently, an empirical parameter γ was introduced in the π-electron model to account for the *curvature* effect which not only changes the *overlap* between π orbitals but also causes *mixing* between π and σ orbitals.[15] For a (*n*,0) SWNT, the energy band gap was given by

$$E_g = \frac{2\pi}{\sqrt{3}}t_0\left[\frac{1}{n} + (-1)^{n \bmod 3}\gamma\frac{2\pi}{\sqrt{3}}\frac{1}{n^2}\right] \tag{1}$$

with t_0=2.53 eV, γ=0.43,[16] or γ=1/12 for the π-electron model.[13,15] Tight-binding predictions formed the basis for identification of chirality and interpretation of experimental results[17] to show that SWNTs follow two distinct trends depending on (*n*−*m*)mod 3=1 or 2. Later, a *first-principles* generalized gradient approximation (GGA) study[16] reported significant deviations from the simple tight-binding predictions for tubes with radius smaller than 3.5 Å (*n*=7,8) but confirmed results for larger *n*. The band gap for *n* mod 3 =2 class is found to be higher than the other class.[16] D'yachkov and Hermann[18] used a linear augmented cylindrical wave method to show that E_g in SWNTs is oscillatory in nature depending on *n* mod 3=1 or 2 but reached opposite conclusions for the two classes; the *n* mod 3=1 class has larger gaps than the *n* mod 3=2. Fantini *et al.*[19,20] determined the electronic transition energies of several nanotubes with different chiralities based on resonant Raman spectroscopy and confirmed the existence of two classes of SWNTs, depending on (2*n*+*m*)mod 3 equal to 1 or 2, respectively. Telg *et al.*[21,22] also reported the evidence of two classes of SWNTs based on (*n*−*m*)mod 3; they interpreted their results based on three nearest-neighbor tight-binding model.[23] A comprehensive first-principles study of 40 different small

diameter SWNTs,[24] employing density-functional theory (DFT) within the local-density approximation (LDA), confirmed the deviation from a simple $1/d$ behavior and explained the existence of two families of semiconducting SWNTs: the mod 2 gaps are larger than the mod 1 gaps for two consecutive n values. Later, however, a first-principles plane-wave density-functional calculation reported again a monotonic decrease in E_g for SWNTs (Ref. [25]) from (10,0) to (17,0).

Using two-photon excitation spectroscopy[26] and combining electron diffraction with Rayleigh scattering,[27] it has been confirmed that E_g (and higher-order transition energies) is consistently lower for mod 1 than for mod 2 tubes. Under strain, this chirality dependence of the transitions leads to opposite shifts in band gap energies for these two families.[28] For zigzag SWNTs, the tight-binding result for the change in band gap ΔE is simply $\pm 3t_0(1+\nu)\sigma$ (positive for n mod 3 =1 and negative for n mod 3=2). σ is the uniaxial strain and ν is the Poisson ratio which takes into account homogeneous deformation perpendicular to the strain axis. For the commonly used values $t_0=2.7$ eV and $\nu=0.2$, one obtains ΔE as ± 97 meV per 1% strain. Experimental measurements which employ an atomic force microscope (AFM) seem to be consistent[29,30] with the ± 100 meV range per 1% strain. Using Rayleigh scattering spectroscopy, however, the strain-induced shifts were found to be almost a factor of 2 *smaller*.[31] These are important issues central to the correct assignment of chirality indices to SWNTs. It is therefore timely to study the gap behavior and strain-induced changes using a self-consistent and systematic approach.

The rest of the paper is organized as follows. A brief description of the theoretical approach is described in Sec. II. Results and discussions are presented in Sec. III followed by a short summary in Sec. IV.

II. METHOD

Our calculations are performed using the periodic density-functional method, which involves GGA for the exchange and correlation within the framework of the Perdew-Wang 91 formalism.[32,33] We have used the Vienna *ab initio* Simulation Package (VASP) (Ref. [34]) to carry out the calculations. To construct the $(n,0)$ nanotube structure within the periodic approach, we placed the unit cell of the SWNT in a tetragonal lattice with the tube parallel to the z axis. The lattice parameter was varied from 4.25 to 4.28 Å to find the optimal z translation based on minimal total energy. The other two sides of the unit cell are chosen in such a way that the interwall distance between the tubes for different diameter is kept fixed at ~ 11 Å. This large interwall separation is used to ensure negligible interaction between the nanotube and its images along x and y directions. We have used $1\times 1\times 7$ k-point mesh (Monkhorst-Pack) for the determination of equilibrium geometry of SWNT. A stringent force criterion of 0.01 eV/Å is used for individual atoms during the full structural relaxation. The convergence threshold for energy is taken to be 10^{-6} eV. We have tested the convergence for E_g with respect to the choice of k-point sampling; for example, in the case of (8,0) SWNT, a $1\times 1\times 1$ k point (one irreducible k point) predicts a 0.7242 eV band gap, a $1\times 1\times 7$ k-point (four irreducible k points) mesh yielded 0.591 eV for the E_g, which is changed to 0.5904 eV with $1\times 1\times 11$ k-point mesh (seven irreducible k points). Considering the excellent convergence obtained with higher k-point sampling, one can clearly conclude that at least four irreducible k points are required to obtain accurate picture of the energy band gap and equilibrium structure. The plane-wave cutoff is taken to be 286.74 eV and kept fixed for all SWNT with different diameters.

In a simple tight-binding model, the changes in band gap and higher-order transition energies can be determined from quantized slices of the two-dimensional (2D) graphene band structure and the **K**-point shift due to strain. The change in band gap ΔE induced by uniaxial strain σ is given by[28]

$$\Delta E = \text{sgn}(2p+1)3t_0(1+\nu)\cos(3\theta)\sigma. \quad (2)$$

The factors $p=0$ (metallic) and ± 1 (semiconducting) satisfy $p=n-m-3q$, with q being an integer and (n,m) characterizes the SWNT. Homogeneous deformation perpendicular to the strain axis is taken into account in this model by the Poisson ratio ν. For zigzag SWNTs ($m=0$, $\theta=0$), ΔE is simply $\pm 3t_0(1+\nu)\sigma$ (positive for n mod 3=1 and negative for n mod 3=2). To describe shifts in higher-order transition energies ΔE_{kk}, Eq. (2) is multiplied by $(-1)^{k+1}$ (successive lines originate from lines on alternating sides of the **K** point[31]).

Combining Eqs. (1) and (2) one obtains the strain-dependent transition energies [the band gap is $E_{11}(\sigma)$; terms of $O(n^2)$ have been neglected for the sake of simplicity]

$$E_{11}(\sigma) = E_g + \Delta E = 2t_0[\pi/(\sqrt{3}n) - (-1)^{n \bmod 3}3/2(1+\nu)\sigma], \quad (3a)$$

$$E_{22}(\sigma) = 2t_0[2\pi/(\sqrt{3}n) + (-1)^{n \bmod 3}3/2(1+\nu)\sigma]. \quad (3b)$$

A semiconductor-metal transition ($E_{11}=0$) occurs for $\sigma_{met}=(-1)^{n \bmod 3}2\pi/[3\sqrt{3}n(1+\nu)]$ which gives 5% strain for a (20,0) SWNT with $\nu=0.2$. The maximum gap is obtained when $E_{11}(\sigma_{max})=E_{22}(\sigma_{max})$ or $\sigma_{max}=-(-1)^{n \bmod 3}\pi/[3\sqrt{3}n(1+\nu)]$. Therefore, $|\sigma_{met}|=2|\sigma_{max}|$ and the maximum gap is $E_{11}(\sigma_{max})=3/2E_g$. It also follows that $\sigma_{met}(2n,0)=\sigma_{max}(n,0)$, e.g., the semiconductor-metal transition for a (20,0) SWNT takes place under the same strain value for which the (10,0) gap maximum occurs. Later, these tight-binding results will be compared to self-consistent-field (SCF) results with full geometry optimization.

III. RESULTS AND DISCUSSIONS

A. Band gaps as a function of diameter

Figure 1 shows the results for Kohn-Sham direct energy band gap as a function of their diameter, indicating deviation from a simple monotonic decrease in E_g with increase in diameter of the SWNT. Up to (8,0), the strong curvature distortion changes the simple picture derived from the properties of graphene. From (10,0) onward, the trend in E_g can be explained surprisingly well with the simple relation de-
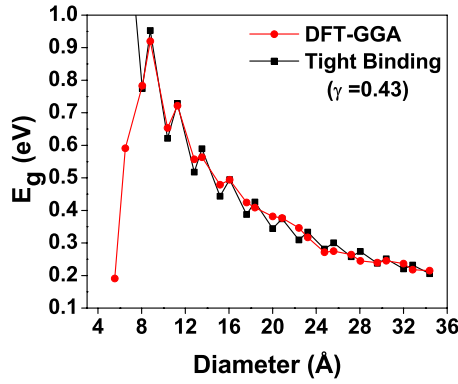
FIG. 1. (Color online) Energy band gap (E_g) as a function of the diameter for $(n,0)$ zigzag nanotubes; the line with solid circles shows the predictions from DFT (GGA) and the line with solid squares represents predictions from a tight-binding model with a parameter $\gamma = 0.43$.

rived from the tight-binding calculation that accounts for the trigonal shape of the equienergy lines around the **K** point and models σ-π mixing with the empirical parameter $\gamma = 0.43$ in Eq. (1). Due to trigonal warping, Eq. (1) predicts that the energy band gap for mod 1 class is reduced (k_{vic} is the point in the projected BZ of graphene closest to **K** point which determines the gap in SWNT and approaches **K** from the **M** point outside the first BZ). In the case of mod 2 class the gap becomes larger (k_{vic} approaches **K** from Γ point). Our first-principles calculations confirm that the $(n,0)$ SWNTs fall into two classes depending upon $n \bmod 3 = 1$ (smaller band gaps) or 2 (larger gaps). The amplitude of the gap oscillations, enhanced through the curvature induced σ-π mixing, decreases from (10,0) to (17,0). From $n = 19$ onward, corresponding to a radius larger than ~ 15 Å, the gap roughly follows the $1/d$ behavior with only a minor deviation predicted by the π-electron model with $\gamma = 1/12$ in Eq. (1). Within each class of SWNT, the E_g decreases monotonically with increasing diameter beyond the initial curvature dominated region ($n < 10$).

Figure 2 shows the energy-band structures for three representative SWNTs. The energy bands around the Fermi energy are doubly degenerate and primarily π and π^* in nature for the valence and conduction bands, respectively. We ana-
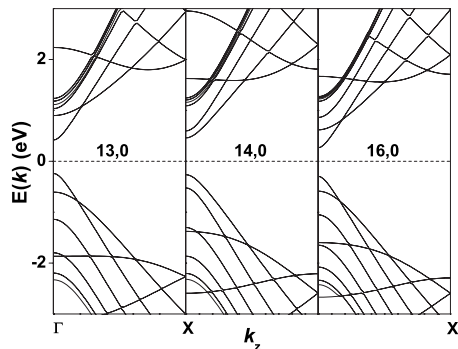

FIG. 2. Energy-band structure of three representative SWNTs (13,0), (14,0), and (16,0). The dotted line at zero represents the Fermi energy level.
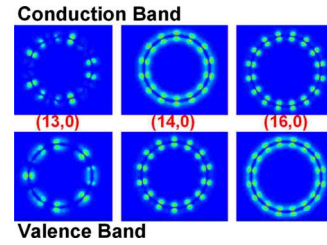

FIG. 3. (Color online) Band decomposed charge density at the Γ point for (13,0), (14,0), and (16,0).

lyzed the band decomposed charge density at the Γ point for the three SWNTs (Fig. 3). It can be seen from the Fig. 3 that the valence bands in (13,0) and (16,0) show a bonding character with electron cloud smeared between atoms along the circumference [more evident in (16,0)]. The conduction bands in this class ($n \bmod 3 = 1$) show antibonding character with electron clouds highly localized around the atoms. In the case of (14,0), i.e., $n \bmod 3 = 2$ class shows an opposite trend of localized electron cloud in the valence band and smeared in the conduction band. It is also evident that (13,0) exhibits more $\sigma - \pi$ mixing than the other two SWNTs of larger diameters as predicted from Eq. (1).

Table I summarizes our results together with the values reported in the literature for E_g in SWNT. The first row represents E_g calculated in the current study. Our GGA gaps are in excellent agreement with the LDA gaps reported in Ref. 24, as one could expect for carbon-based materials. They are also in good agreement with the values reported for (7,0) to (14,0) of Ref. 16; LDA result for (8,0) of Ref. 35; and (10,0) and (11,0) of Refs. 13 and 15. Also, our results match qualitatively for (10,0) to (14,0) of Ref. 2. We believe that the absence of band gap oscillation reported in Ref. 25 is a consequence of nonoptimal z translation leading to spurious strains in SWNTs. It should be noted that the trend in E_g obtained from a crude single k-point sampling of the BZ during structural optimization will yield persistent oscillations of E_g from $n = 11$ onward, as observed in Ref. 18. The discrepancy between the current results and the tight-binding values reported for (7,0) and (8,0) (Refs. 2, 15, and 35) can be attributed to the strong curvature effect that is not included in these tight-binding models. The first experiments that probed the relationship between electronic properties and structure of SWNTs reported band gap values whose distribution could be fitted with the simple tight-binding expression $E_g = 2t_0 a_{CC}/d$ with $t_0 = 2.45$ (Ref. 8) and 2.7 eV,[9] respectively, and d as the tube diameter. Selected experimental values corresponding to our calculation are given in Table I. The agreement is reasonable and within the uncertainty of precisely determining the diameter and corresponding chirality angle, i.e., (n,m) of a given SWNT.

B. Strain-induced changes in the band gaps

We have varied the lattice parameter along the axis of the SWNTs from 4.25 to 4.28 Å to find the influence of longitudinal strain on E_g (Fig. 4). As predicted by the tight-binding Eqs. (3a) and (3b), E_g for the two different classes of SWNTs is found to exhibit opposite trends; the band gap for

TABLE I. Energy band gap (E_g) as a function of n of zigzag SWNTs. The first row under *Ab initio* presents the data from the current study obtained from DFT GGA.

n	7	8	10	11	13	14	16	17
				Ab initio				
E_g	0.19	0.59	0.78	0.92	0.65	0.72	0.56	0.56
Ref. 24	0.21	0.59	0.77	0.93	0.64	0.72	0.54	0.58
Ref. 25	0.48	0.57	0.91	0.77	0.72	0.63	0.61	0.53
Ref. 16	0.24	0.64	0.75	0.94	0.63	0.74		
Ref. 35	0.09	0.62						
				Tight binding				
Ref. 15	1.11	1.33	0.87	0.96				
Ref. 35	1.04	1.19						
Ref. 2	1	1.22	0.86	0.89	0.69	0.7		
				Expt.				
Ref. 8			0.9 ± 0.05[a]	0.8 ± 0.05[a] 0.75 ± 0.05[a]				
Ref. 9							0.5 ± 0.05[b]	0.55 ± 0.05[bc]

[a]Data obtained from Fig. 3(c) of Ref. 8.
[b]Data obtained from Table 1 of Ref. 9.
[c]Reported chiral angle of 25° and accuracy of ~1°; 30° corresponds to a zigzag tube.

n mod $3=1$ increases with an increase in the z-axis translation. For n mod $3=2$, the band gap is found to decrease with the increase in z translation. Again this reinforces the existence of two distinct classes of SWNTs. It also suggests that an optimal z translation is crucial for obtaining correct feature of the E_g.

For (10,0) and (20,0) tubes, the potential surface and band gap changes were explored up to approximately $\pm 6\%$ strain or compression. For each strain value, *full internal geometry relaxation was allowed*. The resulting potential curve for the (20,0) carbon nanotube is shown in Fig. 5(a). It can be seen that a parabola is an excellent fit for the SCF energies with only small deviations occurring for strains larger than $4-5\%$, i.e., Hooke's law is fulfilled over a large range of strains. The potential minimum ($\sigma=0\%$) is found for $z =4.27$ Å. From the second derivative of the "SCF" (20,0) potential curve [Fig. 5(a)], we calculate Young's modulus of
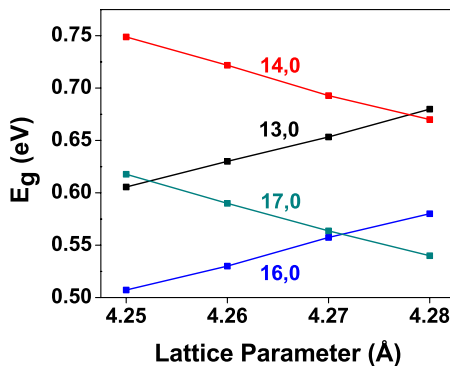
1035 GPa (973 GPa for the "quadratic fit" curve which uses only points up to 4% strain for the parabolic least square fit) assuming a wall thickness of 3.4 Å (twice the van der Waals radius of C). Virtual identical results are obtained for the (10,0) SWNT (1037 and 979 GPa, respectively). These calculated values are in excellent agreement with the experimental results just published:[36] an average Young's modulus of 0.97 ± 0.16 TPa was reported for the SWNTs investigated, independent of the nanotube chiral index.

The calculated SCF band gap changes for the (10,0) and (20,0) SWNTs are shown in Fig. 5(b). They exhibit qualitatively the behavior predicted from Eqs. (2) and (3), i.e., changes in optical transition energies determined from quantized slices of the 2D graphene structure and from the **K**-point shift due to strain. These tight-binding transition energies are shown for $n=20$ [Fig. 5(b)] using $t_0=2.7$ eV and $\nu=0.2$. The (20,0) SCF slope $d\Delta E/d\sigma$ is $\pm (115 \pm 10)$ meV; for the (10,0) SWNT, $d\Delta E/d\sigma$ is 113 meV for $-4\% \le \sigma \le +4\%$. Both are about 10% *larger* than the tight-binding result of ± 97 meV per 1% strain. The semiconductor-metal transition for the (20,0) SWNT is found for $\sigma=3.7\%$ ($z =4.43$ Å) at the strain value for which the (10,0) gap maximum is found, consistent with the tight-binding relation $\sigma_{met}(2n,0)=\sigma_{max}(n,0)$ discussed before. The (20,0) gap reaches its maximum for $\sigma=-1.6\%$ ($z=4.20$ Å) and then decreases. In our calculation, it reaches zero again for $\sigma= -7.5\%$ ($z=3.95$ Å; outside of Fig. 5).

The V shape of the band gap change can be understood easily from the zone-folding picture. In Fig. 6, the dotted lines around the **K** point of the graphene BZ represent two of the available states consistent with the boundary condition for a $(n,0)$ zigzag nanotube with n mod $3=1$ [Fig. 6(a)] and n mod $3=2$ [Fig. 6(b)]. They are spaced by a distance d

FIG. 4. (Color online) Energy band gap (E_g) as a function of the lattice parameter along the z axis of the SWNT.
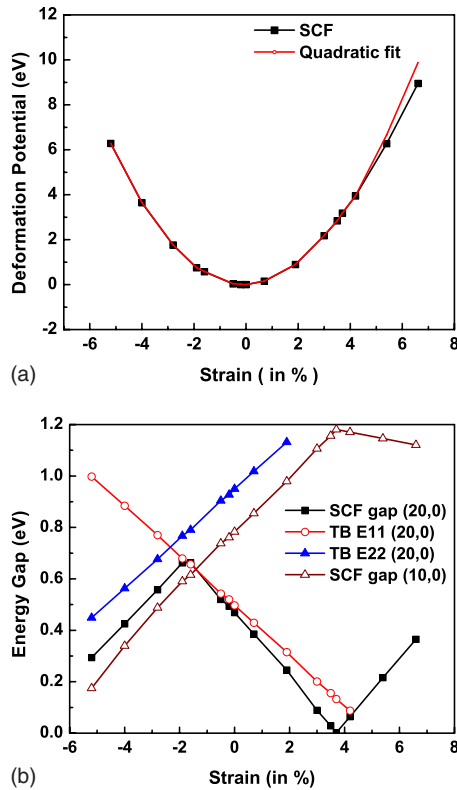
FIG. 5. (Color online) (a) Deformation potential (relative SCF binding energy) as a function of strain for the (20,0) SWNT (black squares). A parabola (red line online) is an excellent fit for the SCF energies with only small deviations occurring for strains larger than 5%, i.e., Hooke's law is fulfilled over a large range of strains. The minimum of the potential ($\sigma=0$) is found for $z=4.27$ Å. (b) Calculated SCF band gap changes for the (10,0) and (20,0) SWNTs as a function of strain. For (20,0) SWNT, the SCF gap change is compared to the tight-binding changes predicted by Eq. (2). The SCF slope $d\Delta E/d\sigma$ for (20,0) SWNT is $\pm(115\pm10)$ meV, about 10% larger than the tight-binding result of ±97 meV per 1% strain.

$=2\pi/na_0$. The distance d_G to **K** which defines the band gap is $1/3d$ for E_{11} and $2/3d$ for E_{22}, respectively. Under axial strain, the **K** point moves *toward* Γ. Therefore, for n mod 3=1, **K** moves *away* from E_{11}. This increases d_G and therefore the gap until the midpoint between the two lines and the gap maximum is reached ($\sigma=3.7\%$ for $n=10$). If the strain is further increased, the gap then becomes defined by
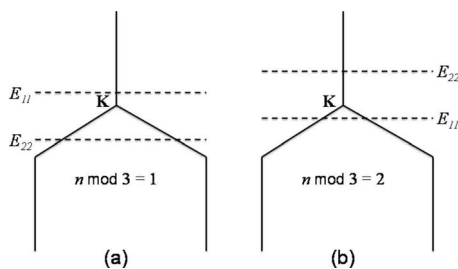

FIG. 6. Two of the available states consistent with the boundary condition for a $(n,0)$ zigzag nanotube with (a) n mod 3=1 and (b) n mod 3=2 in the zone-folding picture around the **K** point of the graphene Brillouin zone.

E_{22} which has now the shorter distance to **K**. For n mod 3 =2, **K** moves *toward* E_{11}; the distance to **K** and therefore the gap decrease under strain until the **K** point reaches E_{11} and the SWNT becomes metallic ($\sigma=3.7\%$ for $n=20$). Under compression, the **K** point moves *away* from E_{11}; the distance to E_{11} and hence the gap increase until the midpoint is reached ($\sigma=-1.6\%$), after which the gap becomes defined by E_{22} and decreases under further compression until it reaches zero once more when **K** reaches E_{22}. For the (20,0) SWNT the symmetry of the V shape as predicted in the tight-binding model is well confirmed by our *ab initio* SCF calculations. For (10,0) the rate of decrease in the gap after the maximum at 3.7% is smaller than the rate of increase for strains below 3.7%. Curvature effects probably distort the symmetry.

In a recent paper, Huang *et al.*[31] used Rayleigh scattering spectroscopy to identify the nanotube crystal structure as well as to measure the effect of strain on the optical transition energies in SWNTs. The axial strain on the SWNT is calculated from the differential thermal expansion between steel and the Si substrate onto which thin gold metal layers "glue" the nanotubes. The strain-induced shifts were found to be almost a factor of 2 *smaller* than that predicted by Eq. (2). The authors showed that inclusion of internal sublattice relaxation in the tight-binding model yields a prefactor of $12\alpha/(1+6\alpha)$ to Eq. (2) which is 0.57 if a previously estimated α value of 0.066 is used, which would explain their experimentally observed shifts not only qualitatively but also quantitatively. The corrected shift for zigzag chains with this prefactor is ±55 meV (instead of ±97 meV) per 1% strain. Earlier experimental measurements on band gap changes in SWNTs employing an AFM (Refs. 29 and 30) which does not require attached electrodes are consistent with the ±100 meV range per 1% strain, confirmed by our *ab initio* calculations with full geometry relaxation. An analysis of the geometry of the converged optimized SCF structures did not show any difference in deformation between the two triangular sublattices; under strain, the equilateral triangles with $a_0=\sqrt{3}d_{CC}$ become elongated in the same way. For example, under 3.75% strain, the long arm of the isosceles triangle is 2.531 Å and the base a_0 is shortened from 2.456 to 2.442 Å by a factor of 0.9943 which corresponds to a Poisson ratio ν of 0.152 to obtain an equivalent shrinking with the tight-binding factor $(1-\sigma\nu)$. The optical transitions measured in Ref. 31 are excitonic in nature. It will need further investigations whether excitonic transitions behave differently under strain than band transitions to explain the difference in shifts in transition energies.

IV. SUMMARY AND CONCLUSIONS

In summary, we have used *ab initio* gradient corrected density-functional computations to investigate the diameter dependence of E_g and strain-induced changes in E_g of SWNTs. The SCF results with full internal geometry relaxation unambiguously confirm the existence of two classes of SWNT based on n mod 3 equal to 1 (smaller E_g and strain-induced gap *increase*) or 2 (larger E_g and strain-induced gap *decrease*). For (10,0) and (20,0) tubes, the potential surface and band gap changes are explored up to approximately

$\pm 6\%$ strain or compression. The calculated band gap changes are $\pm(115 \pm 10)$ meV per 1% strain, positive for the mod 1, and negative for the mod 2 family, about 10% larger than the tight-binding result of ± 97 meV. Young's modulus of ~ 1000 GPa is calculated. The semiconductor-metal transition for a (20,0) carbon nanotube is found for $\sigma = 3.7\%$. For $n \geq 10$, i.e., for diameters larger than ~ 8 Å (at smaller diameters, strong curvature effects dominate the E_g behavior), the simple tight-binding model explains quite well the results of the fully self-consistent calculations if the trigonal shape of the equienergy lines around the **K** point is properly taken into account.

[1] S. Iijima, Nature (London) **354**, 56 (1991).

[2] N. Hamada, S. I. Sawada, and A. Oshiyama, Phys. Rev. Lett. **68**, 1579 (1992).

[3] J. W. Mintmire, D. H. Robertson, and C. T. White, J. Phys. Chem. Solids **54**, 1835 (1993).

[4] C. T. White, D. H. Robertson, and J. W. Mintmire, Phys. Rev. B **47**, 5485 (1993).

[5] R. A. Jishi, D. Inomata, K. Nakao, M. S. Dresselhaus, and J. Dresselhaus, J. Phys. Soc. Jpn. **63**, 2252 (1994).

[6] M. S. Dresselhaus, G. Dresselhaus, and R. Saito, Carbon **33**, 883 (1995).

[7] R. Saito, G. Dresselhaus, and M. S. Dresselhaus, *Physical Properties of Carbon Nanotubes* (World Scientific, Singapore, 1998).

[8] T. W. Odom, J. L. Huang, P. Kim, and C. M. Lieber, Nature (London) **391**, 62 (1998).

[9] J. W. G. Wildöer, L. C. Venema, A. G. Rinzler, R. E. Smalley, and C. Dekker, Nature (London) **391**, 59 (1998).

[10] Z. Zhang and C. M. Lieber, Appl. Phys. Lett. **62**, 2792 (1993).

[11] P. Kim, T. W. Odom, J.-L. Huang, and C. M. Lieber, Phys. Rev. Lett. **82**, 1225 (1999).

[12] R. Saito, G. Dresselhaus, and M. S. Dresselhaus, Phys. Rev. B **61**, 2981 (2000).

[13] H. Yorikawa and S. Muramatsu, Solid State Commun. **94**, 435 (1995).

[14] S. Reich and C. Thomsen, Phys. Rev. B **62**, 4273 (2000).

[15] H. Yorikawa and S. Muramatsu, Phys. Rev. B **52**, 2723 (1995).

[16] O. Gulseren, T. Yildirim, and S. Ciraci, Phys. Rev. B **65**, 153405 (2002).

[17] S. M. Bachilo, M. S. Strano, C. Kittrell, R. H. Hauge, R. E. Smalley, and R. B. Weisman, Science **298**, 2361 (2002).

[18] P. N. D'yachkov and H. Hermann, J. Appl. Phys. **95**, 399 (2004).

[19] C. Fantini, A. Jorio, M. Souza, M. S. Strano, M. S. Dresselhaus, and M. A. Pimenta, Phys. Rev. Lett. **93**, 147406 (2004).

[20] C. Fantini, A. Jorio, M. Souza, L. O. Ladeira, A. G. Souza Filho, R. Saito, Ge. G. Samsonidze, G. Dresselhaus, M. S. Dresselhaus, and M. A. Pimenta, Phys. Rev. Lett. **93**, 087401 (2004).

[21] H. Telg, J. Maultzsch, S. Reich, F. Hennrich, and C. Thomsen, Phys. Rev. Lett. **93**, 189901(E) (2004).

[22] H. Telg, J. Maultzsch, S. Reich, F. Hennrich, and C. Thomsen, Phys. Rev. Lett. **93**, 177401 (2004).

[23] S. Reich, J. Maultzsch, C. Thomsen, and P. Ordejon, Phys. Rev. B **66**, 035412 (2002).

[24] V. Zólyomi and J. Kürti, Phys. Rev. B **70**, 085403 (2004).

[25] B. Kozinsky and N. Marzari, Phys. Rev. Lett. **96**, 166801 (2006).

[26] G. Dukovic, F. Wang, D. Song, M. Y. Sfeir, T. F. Heinz, and L. E. Brus, Nano Lett. **5**, 2314 (2005).

[27] G. M. Y. Sfeir, T. Beetz, F. Wang, L. Huang, X. M. H. Huang, M. Huang, J. Hone, S. O'Brien, J. A. Misewich, T. F. Heinz, L. Wu, Y. Zhu, and L. E. Brus, Science **312**, 554 (2006).

[28] L. Yang and J. Han, Phys. Rev. Lett. **85**, 154 (2000).

[29] E. D. Minot, Y. Yaish, V. Sazonova, J.-Y. Park, M. Brink, and P. L. McEuen, Phys. Rev. Lett. **90**, 156401 (2003).

[30] J. Heo and M. Bockrath, Nano Lett. **5**, 853 (2005).

[31] M. Huang, Y. Wu, B. Chandra, H. Yan, Y. Shan, T. F. Heinz, and J. Hone, Phys. Rev. Lett. **100**, 136803 (2008).

[32] J. P. Perdew, J. A. Chevary, S. H. Vosko, K. A. Jackson, M. R. Pederson, D. J. Singh, and C. Fiolhais, Phys. Rev. B **46**, 6671 (1992).

[33] J. P. Perdew and Y. Wang, Phys. Rev. B **45**, 13244 (1992).

[34] Vienna *ab initio* Simulation Package, Technische Universität Wien, 1999; G. Kresse and J. Furthmüller, Phys. Rev. B **54**, 11169 (1996).

[35] X. Blase, L. X. Benedict, E. L. Shirley, and S. G. Louie, Phys. Rev. Lett. **72**, 1878 (1994).

[36] Y. Wu, M. Huang, F. Wang, X. M. Huang, S. Rosenblatt, L. Huang, H. Yan, S. P. O'Brien, J. Hone, and T. F. Heinz, Nano Lett. **8**, 4158 (2008).